Catalysis Today 169 (2011) 75–84

Contents lists available at ScienceDirect

Catalysis Today

journal homepage: www.elsevier.com/locate/cattod

Improvement of catalyst stability during methane dehydroaromatization (MDA) on Mo/HZSM-5 comprising intracrystalline mesopores

A. Martínez[a,*], E. Peris[a], M. Derewinski[b,**], A. Burkat-Dulak[b]

[a] Instituto de Tecnología Química, UPV-CSIC, Avda. de los Naranjos s/n, 46022 Valencia, Spain
[b] Institute of Catalysis and Surface Chemistry, Polish Academy of Sciences, 30-239 Krakow, Niezapominajek 8, Poland

ARTICLE INFO

Article history:
Received 15 June 2010
Received in revised form 2 November 2010
Accepted 4 November 2010
Available online 5 January 2011

Keywords:
Methane dehydroaromatization
Mo/HZSM-5
Intracrystalline mesopores
Catalyst stability

ABSTRACT

A new Mo/HZSM-5 catalyst (3 wt% Mo, Si/Al = 26) comprising a carbon-templated zeolite having intracrystalline mesopores sizing ca. 10–20 nm (HZSM-5-BP) has been prepared. For comparison purposes, an equivalent catalyst has also been prepared from a commercial zeolite (HZSM-5-ref). The materials have been extensively characterized by XRD, ICP-OES, N_2 physisorption, SEM-TEM, ^{27}Al MAS NMR, FTIR-pyridine, NH_3-TPD, H_2-TPR, TG-DTG analyses and TPO, and their catalytic activity evaluated for methane dehydroaromatization (MDA) at 700 °C, 1 bar, and 1500 ml/g_{cat} h. The hierarchical Mo/HZSM-5-BP catalyst displayed a lower deactivation rate during MDA than the reference one, leading to a higher and stable aromatics yield at T.O.S. above 3 h, despite a higher amount of less reactive coke (associated to the zeolite acid sites) was produced in the former. We hypothesize that the enhanced tolerance to carbon deposits of the carbon-templated zeolite could be related to the intracrystalline mesopores acting as a trap for coke molecules and leaving a higher fraction of acid sites within the channels active for aromatization.

1. Introduction

The direct conversion of methane, the major component of natural gas, to fuels and high-valued petrochemicals still remains one of the major challenges in the field of heterogeneous catalysis [1]. Oxidative processes such as partial oxidation of methane (POM) to methanol and/or formaldehyde and oxidative coupling of methane (OCM) to mainly ethylene have attracted the interest of many researchers in the last decades. However, up to now, none of these processes have been industrially implemented as the over-oxidation of the wanted products (which are much more reactive than the methane itself) into carbon oxides and water becomes kinetically favoured at increasing methane conversions, resulting in too low per pass yields to make the processes economically viable. There is, then, a strong incentive for developing non-oxidative methane conversion processes that might overcome the limitations of the oxidative ones. In this respect, the non-oxidative methane dehydroaromatization (MDA) has attracted the interest of researchers since the group of Prof. Wang reported for the first time in 1993 the formation of benzene with high selectivity over Mo/HZSM-5 catalysts [2]. An additional advantage of the MDA process is the co-production, besides aromatics, of hydrogen that can be used for fuel cells.

The MDA process suffers, however, from several shortcomings that impose serious limitations to its possible commercialization. One of them is that the reaction is limited by thermodynamics, with equilibrium methane conversions of around 12% to a nearly equimolar mixture of benzene and naphthalene at 700 °C and atmospheric pressure, which are typical conditions for MDA. The other major drawback of MDA is the fast deactivation of the catalyst with time-on-stream (T.O.S.) due to the build up of carbon deposits on the catalyst surface during the reaction [3–6]. In this respect, an intense research effort has been devoted in the last years to better understand the role of zeolite acid sites, the nature and location of Mo species and their specific interaction with the zeolitic acid sites, as well as the nature, location, and deactivating effect of different types of coke as an attempt of enhancing the catalyst lifetime, as recently reviewed [5,7–9]. Though different type of carbon species associated to both the Mo sites and the zeolite have been found to form on the catalyst surface during MDA [3,4,10], heavy polyaromatic-type coke formed by consecutive reactions of the primary aromatics on the zeolitic Brønsted acid sites, and particularly on the strongest ones, has been suggested to be the major cause of catalyst deactivation [6,7]. Different approaches have been applied in order to enhance the lifetime of the Mo/HZSM-5 catalyst. Some of them are based on the inhibition of coke formation through the co-feeding of CO/CO_2 [11,12], O_2 [13], and water [14] besides methane. Though the incorporation of a second metal, such as Pt

* Corresponding author.
** Corresponding author. Tel.: +48 508269392; fax: +48 124251923.
E-mail addresses: amart@itq.upv.es (A. Martínez), ncderewi@cyf-kr.edu.pl (M. Derewinski).

0920-5861/$ – see front matter © 2010 Elsevier B.V. All rights reserved.
doi:10.1016/j.cattod.2010.11.063

[15], Fe and Co [16], to the Mo/zeolite catalyst has been shown to be in certain cases beneficial, modification of the textural and acidic properties of the zeolite host through controlled post-synthesis treatments either before or after incorporation of Mo has been the most widely applied strategy aimed at improving the catalyst performance. Effective post-treatments reported in the literature leading to a lower coking tendency and thus to enhanced catalyst lifetime are, for instance, dealumination [17,18], partial exchange of H^+ by alkali metal cations (i.e. Na^+, Cs^+) [19], and surface silanation [20]. In most of these cases, the treatments were aimed at attaining a proper balance between Mo and H^+ sites in the bifunctional Mo/zeolite catalyst, as it is believed that an "excess" of strong Brønsted acid sites promotes the formation of coke on the zeolite surface and thus catalyst decay [21]. The creation of a proper mesoporosity in the zeolite crystallites upon moderate alkali treatment coexisting with the inherent micropores of HZSM-5 has been also shown to be beneficial from the point of view of MDA activity and stability [22]. This is believed to occur by combining the presence of active sites (MoC_x/MoC_xO_y nanoclusters and zeolitic H^+) within the microporous environment favourable for methane aromatization with a faster mass transport rate of the formed aromatics (mostly benzene and naphthalene) in the mesopores thus preventing consecutive condensation reactions that would finally lead to the formation of deactivating carbonaceous species. In a recent work [23], a hierarchical micro-mesoporous ZSM-5 zeolite synthesized by recrystallization of SBA-15 as silica source has been used for preparing Mo/HZSM-5 catalysts displaying enhanced methane conversion and catalyst durability, thus further supporting the key role of the zeolite porous structure during the MDA reaction.

On the other hand, nearly uniform intracrystalline mesovoids can be generated by growing ZSM-5 crystallites around carbon nanoparticles [24] followed by combustion of the carbon template after zeolite crystallization. It is interesting to remark here that, at variance with the type of mesopores generated by alkali treatment or by recrystallization of ordered mesoporous silicas, the voids created by carbon-templated synthesis are mostly located inside the crystallites interconnecting the 10-ring channels of the MFI structure [25], and thus they are not directly accessible from the external zeolite surface. This kind of intracrystalline mesoporosity may impart the zeolite with particular properties in specific applications. For instance, deposition of metal nanoparticles (Pd^0) inside the mesovoids has been shown to prevent its migration and growing on the external zeolite surface leading to improved metal dispersions after reductive treatments and enhanced sulfur resistance [26] as compared to a *conventional* HZSM-5 sample. In the context of MDA, we may hypothesize that such intracrystalline mesovoids can act as a reservoir for the carbon deposits improving the coke tolerance, and thus presumably the catalyst lifetime. This assumption is based on previous observations where the large 12-ring supercages in HMCM-22 zeolite were proposed to act as traps for coke deposits during MDA producing catalysts with better coke tolerance than Mo/HZSM-5 under similar reaction conditions [27]. The results presented here do support the above hypothesis, and the catalyst prepared from the carbon-templated HZSM-5 zeolite is shown to display enhanced stability with T.O.S. with respect to a Mo/HZSM-5 sample comprising a *conventional* zeolite with equivalent Si/Al ratio.

2. Experimental

2.1. Preparation of Mo/HZSM-5 catalysts

A hierarchical micro-mesoporous NaZSM-5 zeolite was synthesized by a carbon-templated approach using monodispersed Black Pearls 2000 of ca. 12 nm mean diameter (BP2000, Cabot Corp.) as the carbon template, following the methodology reported in [25]. Briefly, a gel with the following molar composition was prepared using fumed silica (Cab-O-Sil, Riedel-de Haën), aluminum nitrate nonahydrate ($Al(NO_3)_3{\cdot}9H_2O$, POCh S.A., Poland), tetrapropylammonium bromide (TPABr, Janssen Chimica), sodium hydroxide (NaOH, POCh S.A., Poland) and water as reagents:

$$SiO_2 : 0.16TPABr : 0.025Al(NO_3)_3{\cdot}9H_2O : 0.34NaOH : 14.5H_2O$$

The gel was then mixed with a concentrated suspension of BP2000 particles (mean size of about 12 nm) in a SiO_2/carbon molar ratio of 1:1, and then crystallized under hydrothermal conditions in Teflon-lined autoclaves at 175 °C for 20 h. After crystallization, the solid was washed, dried, and finally calcined at 600 °C for 8 h to remove the organic and carbon material. The protonic form was then obtained by submitting the as-made NaZSM-5 sample to four consecutive ionic exchanges with a 1 M aqueous solution of NH_4NO_3 at 80 °C for 2 h (liquid/solid ratio of 30 ml/g) under stirring. After each NH_4^+ exchange the solid was filtered, extensively washed with distilled water and dried at 80 °C for 2 h. After the last exchange, the dried zeolite was calcined under the flow of air by raising the temperature from ambient to 500 °C at 2 °C/min and kept at this temperature for 6 h. This sample is denoted as HZSM-5-BP.

A *conventional* HZSM-5 sample purchased to Zeolyst Int. (CBV5020) has been used for comparison purposes. This reference zeolite is denoted here as HZSM-5-ref.

Molybdenum-containing catalysts (3 wt% nominal Mo loading) were prepared by incipient wetness impregnation of the acid zeolites with an aqueous solution of ammonium heptamolybdate tetrahydrate (AHM, Merck), followed by drying at 80 °C and calcination in air flow at 500 °C for 6 h. The molybdenum concentration in the AHM impregnating solution was ca. $2.5–2.9 \times 10^{-1}$ M and its pH was about 5.0–5.3 as measured in a Seven Multi pH meter (Metler Toledo). Under these conditions both monomeric $(MoO_4)^{2-}$ and polymeric $(Mo_7O_{24})^{6-}$ species are coexisting in the AHM solution, with a predominance of the latter [28].

2.2. Characterization of materials

The phase purity of the carbon-templated ZSM-5 zeolite was assessed by use of powder X-ray diffraction (XRD) in a Philips X'Pert diffractometer equipped with a graphite monochromator operating at 40 kV and 45 mA using nickel-filtered Cu Kα radiation (λ = 0.1542 nm). XRD measurements were also performed on the calcined Mo/HZSM-5 catalysts in order to check for the presence of crystalline MoO_3 phases.

The chemical composition of the HZSM-5 samples and the corresponding Mo/HZSM-5 catalysts were determined by ICP-OES (Inductively Coupled Plasma-Optical Emission Spectroscopy) in a Varian 715-ES apparatus after dissolution of the solids in an acid mixture of HNO_3:HF:HCl in a 1:1:3 volume ratio.

Textural properties of the zeolites and Mo-containing catalysts were determined by N_2 physisorption at −196 °C on an ASAP-2000 (Micromeritics) equipment. Before measurements the solids were pretreated at 400 °C and vacuum overnight. The specific surface areas were obtained using the BET model and the micropore volume by applying the *t*-plot approach to the adsorption branch of the isotherms. Pore volume distributions were obtained from the corresponding N_2 adsorption isotherms using the BJH formalism.

The acid properties of the zeolites and Mo-containing catalysts were measured by FTIR (Fourier Transform Infrared) spectroscopy of adsorbed pyridine in a Nicolet 710 FTIR apparatus. For the adsorption experiments, self-supported wafers of 10 mg cm^{-2} were prepared and pretreated overnight at 400 °C and 1.33×10^{-2} Pa of dynamic vacuum. Then, 1.5×10^3 Pa of pyridine were admitted to

the IR cell at room temperature and after equilibration the samples were outgassed for 1 h at increasing temperatures (250, 350, and 400 °C). After each desorption step, the spectrum was recorded at room temperature and the background subtracted. The density of Brønsted and Lewis acid sites was calculated from the integrated areas of the bands at ca. 1545 and 1450 cm^{-1}, respectively, using the extinction coefficients reported by Emeis [29]. Complementary acidity data were obtained by temperature programmed desorption of NH_3 (NH_3-TPD) in an Autochem 2910 equipment (Micromeritics) coupled with a quadrupole mass spectrometer (OmniStar from Balzers Intruments). Before adsorption of ammonia, about 100 mg of sample were pretreated at 450 °C as follows: 30 m in O_2, 15 m in Ar, and finally 15 m in He. The NH_3 uptake (i.e. total amount of acid sites) was obtained by introducing calibrated pulses of ammonia at 175 °C until saturation of the sample. The acid strength distribution was measured by desorption of ammonia from 175 °C to 600 °C at a heating rate of 10 °C/min. The signal corresponding to $m/z = 16$ (signal for NH_2^+) was used to obtain the NH_3 desorption profile.

The morphology and size of the ZSM-5 crystallites were determined by scanning electron microscopy (SEM) in a JEOL JSM-6300 microscope. Transmission electron microscopy (TEM) was also performed on the calcined carbon-templated HZSM-5-BP sample in order to ascertain the presence of intracrystalline mesovoids generated upon combustion of the carbon-template nanoparticles. TEM measurements were carried out in a Philips CM-10 microscope operating at 100 kV. Prior to observation by TEM, the samples were ultrasonically dispersed in ethanol and transferred to a holey-carbon coated copper grid (300 mesh).

^{27}Al MAS NMR (Magic-Angle Spinning Nuclear Magnetic Resonance) spectra were recorded at room temperature in a Bruker AV400 spectrometer working at 104.2 MHz, using a 4 mm Bruker BL4 probe. Samples were packed into zirconia rotors and spun at the magic angle spinning (MAS) at 10 kHz. The ^{27}Al spectra were acquired with pulses of 0.5 μs corresponding to a flip angle of $\pi/18$ and were referred to a 0.1 M aqueous solution of $Al(NO_3)_3$.

The reduction behaviour of zeolite-supported molybdenum phases in calcined catalysts was studied by hydrogen temperature-programmed reduction (H_2-TPR) in a Micromeritics Autochem 2910 equipment. About 100 mg of sample were introduced in a quartz cell and flushed with an Ar flow (10 ml/min) at room temperature for 30 min. Then, the gas was switched to the reductive mixture (10 vol% H_2 in Ar, flow rate = 50 ml/min) and the temperature was linearly increased up to 1100 °C at a heating rate of 10 °C/min. The water generated during the reduction was retained in a 2-propanol/N_2(liq.) trap and the H_2 consumption monitored in a thermal conductivity detector (TCD) previously calibrated using the reduction of CuO as reference. No sublimation of metallic Mo species was observed during the H_2-TPR experiments.

For TPO (temperature-programmed oxidation) analysis, the coked catalyst (ca. 100 mg) was first pre-treated in He flow (30 ml/min) at 100 °C for 0.5 h to remove adsorbed water. After cooling to room temperature, a flow of 5 vol% O_2/He (30 ml/min) was established and the temperature linearly increased up to 800 °C at a heating rate of 10 °C/min. The TPO experiments were conducted in a Micromeritics Autochem 2910 analyser comprising a TCD and coupled to a OmniStar quadrupole mass spectrometer (Balzers Intruments) to monitor the evolution of the species with $m/e = 28$ (CO), 18 (H_2O) and 44 (CO_2).

Thermogravimetic and derivative thermogravimetric (TG-DTG) analyses were performed in a Netzch SAT409 EP instrument coupled to a thermobalance. Typically, the charge of coked catalyst was ca. 20 mg and the flow rate of air was 100 ml/min while the temperature was increased from ambient to 800 °C at a heating rate of 10 °C/min.

2.3. Methane dehydroaromatization experiments

Methane dehydroaromatization (MDA) experiments were carried out in a continuous down-flow fixed bed quartz reactor at 700 °C and atmospheric pressure. Typically, 0.4 g of catalyst previously crushed and sieved to a particle size of 0.25–0.42 mm were diluted with 2.0 g of silicon carbide (SiC) and loaded to the reactor. Catalyst dilution with SiC was verified to have no affect on methane conversion and aromatics yield (see Fig. S1 of Supporting information). The catalysts were pre-treated *in situ* in a flow of He (15 ml/min) by raising the temperature from ambient to 700 °C, and kept at this temperature for 30 min. Then, the He flow was switched by the feed gas mixture comprising CH_4 and N_2 (used as internal standard) in a 9:1 volumetric ratio at a flow rate of 10 ml/min, corresponding to a space velocity of 1500 ml/g_{cat} h.

The unconverted methane and the formed carbon-containing products (CO_x, C_2's, and C_6–C_{10} aromatics) were separated and analyzed *on line* at different T.O.S. in a gas chromatograph (HP-GC6890) equipped with two columns (HayeSep Q and Molecular Sieve 5A) and two detectors (TCD and FID). Yields and selectivities to the different products are given on a carbon basis. The amount of carbonaceous deposits was obtained from the *on line* GC analyses as the difference between the carbon in the feed (from CH_4) and in the carbon-containing products (unreacted CH_4, CO_x, hydrocarbons) at the reactor outlet using the N_2 accompanying CH_4 in the feed stream as internal standard.

3. Results and discussion

3.1. Characteristics of ZSM-5 samples

The X-ray diffraction patterns of the HZSM-5 samples and the respective Mo-containing catalysts are shown in Fig. S2 of Supporting information. No diffractions additional to those related to the crystalline MFI structure and no amorphous phases were observed in the as-made NaZSM-5-BP sample. The high crystallinity of HZSM-5-BP can be readily inferred from Fig. S2 by comparing the peak intensities with those of the reference sample.

The chemical composition (Si/Al ratio, Mo loading) determined by ICP-OES, the textural properties derived from N_2 physisorption, and the mean crystallite size (from SEM) for the parent HZSM-5 zeolites and the corresponding Mo-containing catalysts are listed in Table 1. The remaining Na content in HZSM-5-BP was 0.04 wt% (atomic Na/Al ratio of 0.03), indicating that replacement of Na^+ cations in the as-made NaZSM-5-BP sample by NH_4^+ after the four consecutive ionic exchanges proceeded almost quantitatively. As seen in Table 1, the Si/Al ratio of HZSM-5-BP was 26, that is almost the same as the reference one (Si/Al = 25). This value is lower than the Si/Al ratio of 40 in the synthesis gel, which points toward an incomplete incorporation of Si species under the hydrothermal conditions applied in the synthesis of Na-ZSM-BP.

Both the carbon-templated and the reference samples do also show equivalent BET surface areas (379–389 m^2/g) and micropore volumes (0.16 ml/g). As observed in Fig. S3 of Supporting information, the carbon-templated sample shows a broad mesopore volume distribution in the 5–30 range with a maximum for pores of ca. 16 nm in diameter. This value is slightly higher than the mean size of the BP2000 nanoparticles used as carbon template during synthesis (ca. 12 nm), suggesting that some of the carbon particles coupled during synthesis of NaZSM-5-BP leading to larger voids upon combustion. In fact, the representative TEM image shown in Fig. 1 for HZSM-5-BP clearly evidences the presence of voids corresponding to single (10–15 nm) and coupled (20–30 nm) carbon particles. For the sake of clarity, voids originated from single or coupled carbon particles are marked as 1 or 2, respectively, on the

Table 1
Chemical composition and textural properties of HZSM-5 samples and the corresponding Mo/HZSM-5 catalysts.

Sample	ICP-OES		N_2 physisorption		SEM
	Si/Al ratio	Mo (wt%)	BET (m^2/g)	V_{micro} (ml/g)	ACS[a] (μm)
HZSM-5-BP[b]	26	–	389	0.16	0.40 ± 0.20
Mo/HZSM-5-BP	26	3.1	350	0.14	–
HZSM-5-ref	25	–	379	0.16	0.10 ± 0.02
Mo/HZSM-5-ref	25	2.9	358	0.14	–

[a] Average crystallite size.
[b] Remaining Na content = 0.04 wt%.

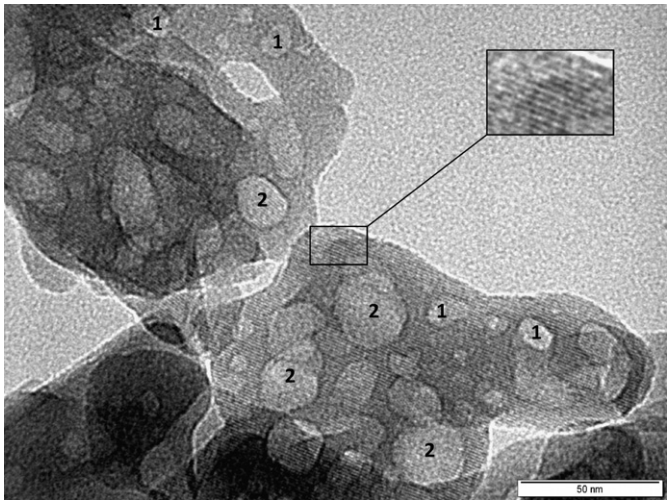

Fig. 1. Representative TEM image of HZSM-5-BP zeolite showing the intracrystalline mesovoids formed upon combustion of single (marked as 1) or coupled (marked as 2) carbon template nanoparticles. The fringes related to the crystalline MFI zeolite structure are clearly perceived in the inset.

TEM image. Moreover, the fringes associated to the crystalline MFI structure are clearly perceived (see magnification in the inset to Fig. 1).

As seen in Table 1, the average crystal size of the carbon template zeolite was ca. 0.4 μm, while the reference sample (commercial CBV5020) comprised smaller crystallites sizing, in average, ca. 0.1 μm. Representative SEM micrographs for the two zeolites are given in Fig. S4 of Supporting information.

The state and coordination of Al species in the zeolites were assessed by ^{27}Al MAS NMR (see Fig. S5 of Supporting information). The spectrum of the as-made Na-ZSM-5-BP zeolite shows only the signal of tetrahedral Al at ca. 54.5 ppm indicating that all the aluminum was effectively incorporated in the zeolite framework during hydrothermal synthesis. The protonic HZSM-5-BP sample shows, in addition to the tetrahedral peak, a weaker contribution at ca. 0 ppm assigned to octahedrally coordinated Al species in extralattice positions pointing toward a partial dealumination of the zeolite framework after the four NH_4^+ exchanges and final calcination at 500 °C. It is worth mentioning that the commercial HZSM-5-ref sample does also displays the weak octahedral feature with similar relative Al^{VI}/Al^{IV} intensity ratio (spectrum not shown).

The acidic properties of the H-zeolites, as determined by FTIR of adsorbed pyridine and NH_3-TPD, are gathered in Table 2. The FTIR spectra in the pyridine region for the two zeolites are shown in Fig. S6 of Supporting information. As seen in the table, both zeolites mostly display Brønsted type acidity (>90% of the total acid sites at a pyridine desorption temperature of 250 °C). The marginal Lewis-type acidity present in the H-zeolites is in agreement with the small contribution from extralattice Al species evidenced by ^{27}Al MAS NMR spectroscopy (Fig. S5). The total amount of Brønsted acid sites (at 250 °C desorption temperature) is alike for the two zeolites (190–207 μmol/g) as expected from the similar bulk Si/Al ratio and Al^{IV}/Al^{VI} NMR intensity ratio, as previously discussed. An alike total amount of acid sites can also be inferred by comparing the NH_3 uptakes (at 175 °C) given in Table 2 (452–457 μmol/g). It can be inferred from the change in the acid site density with increasing pyridine desorption temperature that some of the Brønsted acid sites in the carbon-templated HZSM-5-BP sample are of a somewhat lower strength than in the reference one. In fact, the B_{400}/B_{250} ratio (that is, the ratio between the Brønsted acid sites retaining pyridine at 400 °C and at 250 °C) is 0.46 for HZSM-5-BP and 0.60 for HZSM-5-ref. This result is corroborated by comparing the respective NH_3-TPD profiles (see Fig. S7 of Supporting information). In both cases, a single desorption peak, slightly asymmetric at his left side, is observed though the reference zeolite displays a slightly higher T_{max} value (386 °C against 373 °C in the case of HZSM-5-BP) that supports the FTIR-pyridine results in terms of acid strength distribution. It may be suggested that the slightly weaker Brønsted acid sites in HZSM-5-BP could be those of –OH groups in bridged Si–OH–Al species which are vibrating in the intracrystalline mesopores and thus in a less constrained environment.

3.2. Physicochemical properties of Mo/HZSM-5 catalysts

The Mo content in the two Mo/HZSM-5 catalysts agreed well with the nominal value of 3 wt% (Table 1). As inferred from Fig. S2, the crystallinity of the zeolites was retained to a high extent (>90%) upon impregnation with the Mo precursor's solution and subsequent calcination at 500 °C. No diffraction peaks related to the presence of tridimensional MoO_3 crystallites are detected by this technique in the calcined Mo/HZSM-5 catalysts, indicating a high dispersion degree of Mo oxidic species on the zeolite surface.

Table 2
Acidity of H-zeolites and Mo/HZSM-5 catalysts as determined by FTIR of adsorbed pyridine and NH_3-TPD.

Sample	FTIR-pyridine (μmol/g)							NH_3-TPD	
	Brønsted			B_{400}/B_{250} ratio	Lewis			NH_3 uptake (μmol/g)	T_{max} (°C)
	250 °C	350 °C	400 °C		250 °C	350 °C	400 °C		
HZSM-5-BP	190	150	87	0.46	13	11	8	452	373
HZSM-5-ref	207	162	125	0.60	18	17	17	457	386
Mo/HZSM-5-BP	112	75	43	0.38	14	12	10	318	250, 370
Mo/HZSM-5-ref	67	29	15	0.22	22	12	5	235	250, 325

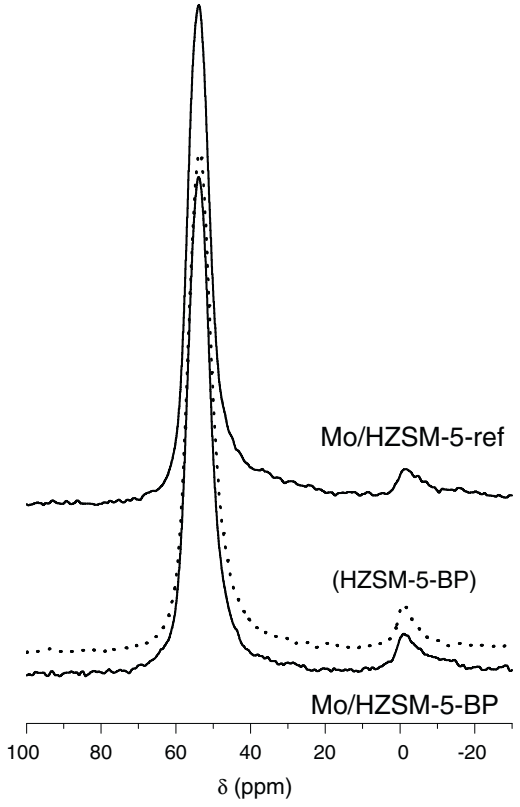

Fig. 2. ^{27}Al MAS NMR spectra of Mo/HZSM-5 catalysts. For comparison, the spectrum of the parent HZSM-5-BP zeolite is also shown (dotted line).

Incorporation of molybdenum produced a small decrease in BET surface area of about 5 and 10% for Mo/HZSM-5-ref and Mo/HZSM-5-BP, respectively (Table 1). Concomitantly, the micropore volume was slightly decreased from 0.16 to 0.14 ml/g. Such a small decrease in surface area and microporosity can be mainly related to the "mass dilution effect" (the nominal oxide content assuming Mo as MoO_3 is 4.5 wt%) though a partial blockage of micropores by the supported MoO_x species is not discarded.

The effect of Mo incorporation on the nature of Al species can be addressed by comparing the ^{27}Al MAS NMR spectra of the parent zeolites, as seen in Fig. S5 of Supporting information, with those of the respective Mo/HZSM-5 catalysts shown in Fig. 2. It is evidenced in Fig. 2 that the nature of Al species is hardly modified with respect to the pure zeolites (in order to make the comparison clearer, the spectrum of HZSM-5-BP has also been included in Fig. 2 as a dotted curve) after incorporation of 3 wt% Mo. Interestingly, no signals associated to extralattice $Al_2(MoO_4)_3$ species are observed for both catalysts. This implies that no further extraction of Al from the zeolite framework occurred during the impregnation and calcination (at 500 °C) steps of catalyst preparation. In fact, a strong interaction between mobile MoO_x species and framework Al leading to the formation of MDA-inactive extraframework $Al_2(MoO_4)_3$ species (characterized by a signal at ca. −13 ppm which shifts to +14 ppm after hydration [30,31]) has been shown to be more favourable with increasing the severity of the thermal treatment [32].

The acidity of the Mo-containing catalysts has also been studied by FTIR-pyridine (see spectra in Fig. S6 of Supporting information) and NH_3-TPD. The quantitative data derived from both techniques are given in Table 2. It is evidenced from both the amounts of pyridine retained at 250 °C and the NH_3 uptakes (at 175 °C) that incorporation of Mo and calcination drastically reduces the amount of acid sites, particularly those of the Brønsted type. It is worthy to note that the relative decrease in acid site density is meaningfully

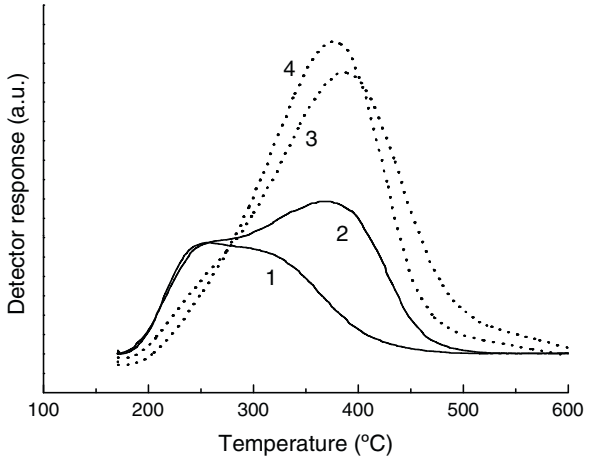

Fig. 3. NH_3-TPD profiles for Mo-containing catalysts and parent zeolites: (1) Mo/HZSM-5-ref; (2) Mo/HZSM-5-BP, (3) HZSM-5-ref; and (4) HZSM-5-BP.

lower for the catalyst comprising the carbon-templated zeolite. Thus, the ratio in the amount of Brønsted acid sites retaining pyridine at 250 °C after and before Mo loading is 0.59 for Mo/HZSM-BP and 0.32 for Mo/HZSM-5-ref. The same trend is evidenced by comparing the NH_3 uptakes for the parent zeolites and the Mo-loaded catalysts. Besides the decrease in Brønsted acid amount, modification with Mo has the effect of decreasing the average strength of the remaining acid sites, as readily inferred from the lower B_{400}/B_{250} ratio values in the Mo/HZSM-5 catalysts as compared to the Mo-free zeolites (Table 2). This effect is more drastic in Mo/HZSM-5-ref, for which the relative proportion of very strong Brønsted acid sites (those retaining pyridine at 400 °C) is about 1/3 of that in the parent zeolite. The change in acid strength distribution upon Mo loading can be better appraised by looking to the NH_3-TPD profiles shown in Fig. 3. There, the profiles of the Mo-free zeolites have also been included as dotted curves in order to better visualize the effects. Clearly, the contribution of the low temperature desorption feature (peaking at 250 °C), evidenced as a weak shoulder in the profiles of the pure zeolites, has been significantly increased in the Mo-containing catalysts while that peaking at higher temperature (>300 °C) has been reduced. Moreover, in line with the FTIR-pyridine results, not only the reduction in the amount of acid sites (inferred from the area under the TPD curves and NH_3 uptakes) has been more severe in Mo/HZSM-5-ref with respect to Mo/HZSM-5-BP but also the incorporation of Mo has decreased to a much greater extent the amount of the stronger sites (those peaking at 386 °C in the parent zeolite) resulting in a shift of T_{max} toward lower temperatures (325 °C, Table 2) in the former catalyst. By contrast, Mo loading has little effect on T_{max} for the high temperature desorption peak in Mo/HZSM-5-BP (370 °C against 373 °C in the parent zeolite).

It has been shown in previous works that part of the MoO_x species (formed by decomposition of the heptamolybdate precursor) can diffuse and migrate from the external surface into the zeolite channels during the calcination step via surface and gas-phase transport, where they can exchange with Brønsted acid sites and remain there anchored [33]. As pointed by Su et al. [34] the Brønsted acid sites are the driving force for the migration of MoO_x into the micropores. According to Iglesia and coworkers the Mo species replace the zeolitic protons in a 1:1 stoichiometry ratio forming di-tetrahedral $(Mo_2O_5)^{2+}$ structures as illustrated in Scheme 1 [33], though it has been recently proposed that the anchoring mode of Mo may be determined by the Si/Al ratio of the zeolite [35]. By using ^{1}H MAS NMR spectroscopy, Liu et al. [36] were able to distinguish between MoO_x species associated and

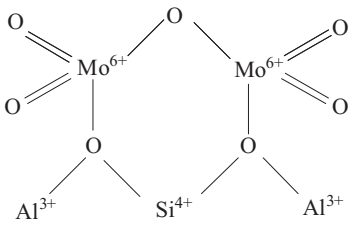

Scheme 1. Proposed structure for the Mo species formed after exchange with zeolite Brønsted acid sites [33].

non-associated with the Brønsted acid sites and concluded that the former are intrinsically more active and stable for the MDA reaction. Recently, direct observation of the active Mo species at the exchange zeolitic sites has been made possible by using ultrahigh field ^{95}Mo NMR spectroscopy [37]. Assuming the Iglesia's model, the higher the extent of migration and interaction with the zeolite acid sites during calcination the lower the amount of remaining acid sites would be. If this is so, the acidity results obtained in the present study suggest that more MoO_x species have migrated into the channels and interacted with Brønsted acid sites in the case of Mo/HZSM-5-ref catalyst as compared to Mo/HZSM-5-BP. Considering the FTIR-pyridine data at a desorption temperature of 250 °C, the amount of Brønsted acid sites upon Mo incorporation and calcination at 500 °C for 6 h was decreased to 32% and 59% for Mo/HZSM-5-ref and Mo/HZSM-5-BP, respectively, with respect to the parent zeolites (Table 2). Since the total amount of Brønsted acid sites (measured after desorbing pyridine at 250 °C) does not differ substantially for the reference and the carbon-templated zeolite, the observed divergence in the extent of migration and interaction of MoO_x species should be related to differences in the porous structure between both zeolites, though further work is in progress in order to provide a plausible explanation for this phenomenon. It may be speculated that the migration of part of Mo into the intracrystalline mesovoids in HZSM-5-BP could reduce the effective amount of Mo species remaining inside the 10-ring channels after calcination. Nonetheless, differences in the crystallite size between the two zeolites could also have an affect on the relative location of Mo.

The reducibility of the catalysts was studied by means of H_2-TPR with the aim of gaining further insight into the location of Mo species and Mo–zeolite interaction in the two studied catalysts. It has been reported on the basis of EPR characterization that Mo species directly interacting with the zeolite inside the channels are more difficult to be reduced by methane that those located on the external surface [38]. In our study, the H_2-TPR experiments were performed on catalysts that were calcined at 500 °C for 6 h and then submitted to a pretreatment in He at 700 °C for 30 min, that is, the same pretreatment which is done *in situ* prior to feeding the CH_4/N_2 mixture to the reactor (see Experimental). The obtained H_2-TPR profiles are shown in Fig. 4. For both catalysts four reduction regions can be identified (see dotted vertical lines): (I) 200–375 °C, (II) 375–560 °C, (III) 560–890 °C, and (IV) 890–1100 °C. The same reduction features, thought with different relative contributions, have been recently reported by Song et al. for 6wt%Mo/HZSM-5 catalysts [39]. According to these authors, the weak reduction feature in region I may be related to the partial reduction of amorphous polymeric molybdate species, region II corresponds to the reduction of MoO_3 to MoO_2 and is the main reduction feature in our samples, and region III is probably due to the complete reduction of Mo^{4+} species to Mo^0. It is interesting to mention that the high temperature reduction region peaking at ca. 1030 °C was reported for the first time in the paper from Song et al. [39] and was not previously observed probably because the final temperature reached in typical H_2-TPR experiments (900 °C) was not high enough to

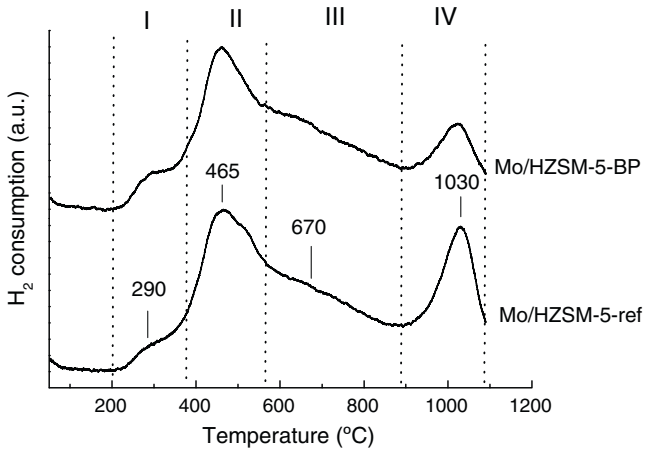

Fig. 4. H_2-TPR profiles for Mo/HZSM-5 catalysts calcined at 500 °C for 6 h and subsequently pretreated in He at 700 °C for 30 min (see text).

observe the reduction of such refractory species. According to Song et al. [39] the high temperature reduction feature in region IV might be assigned to the deep reduction of $(Mo_2O_5)^{2+}$ species located in the zeolite channels. The reduction profiles obtained in the present work are quite similar for the two Mo/HZSM-5 catalysts studied. The most striking difference is, perhaps, a larger relative contribution of the high temperature reduction feature (region IV) for Mo/HZSM-5-ref. According to the assignment proposed in [39] for the reduction feature at ca. 1000 °C, our H_2-TPR results point toward a higher proportion of hardly reducible Mo species located inside the 10-ring channels in Mo/HZSM-5-ref as compared to Mo/HZSM-5-BP. This result concurs well with the observed trend in relative loss of Brønsted acidity upon Mo loading and calcination, as discussed previously.

3.3. Catalytic evaluation for MDA

The change in methane conversion with time-on-stream (T.O.S.) at 700 °C and 1500 ml/g_{cat} h space velocity for the two Mo/HZSM-5 catalysts is shown in Fig. 5. Both catalysts display the typical conversion-T.O.S. trend observed in many previous works for MDA over Mo/HZSM-5, that is, a pronounced decrease in conversion during the initial reaction stages (ca. 3 h under the conditions employed here) due to the rapid buildup of carbonaceous deposits on the catalyst followed by a smoother decrease in conversion at longer times. As seen in the figure, the initial (i.e. at very short T.O.S.)

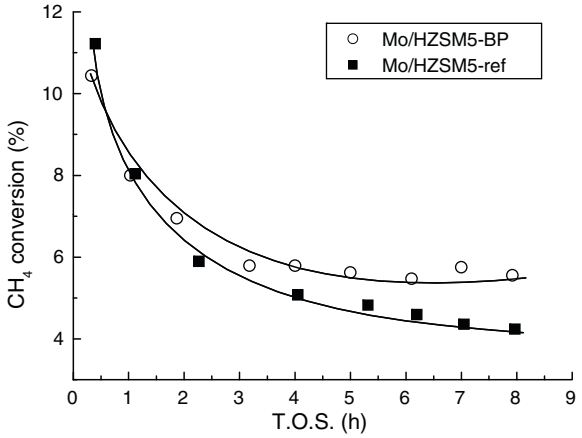

Fig. 5. Change of methane conversion with T.O.S. for Mo/HZSM-5 catalysts at 700 °C, atmospheric pressure, and space velocity of 1500 ml/g_{cat} h.

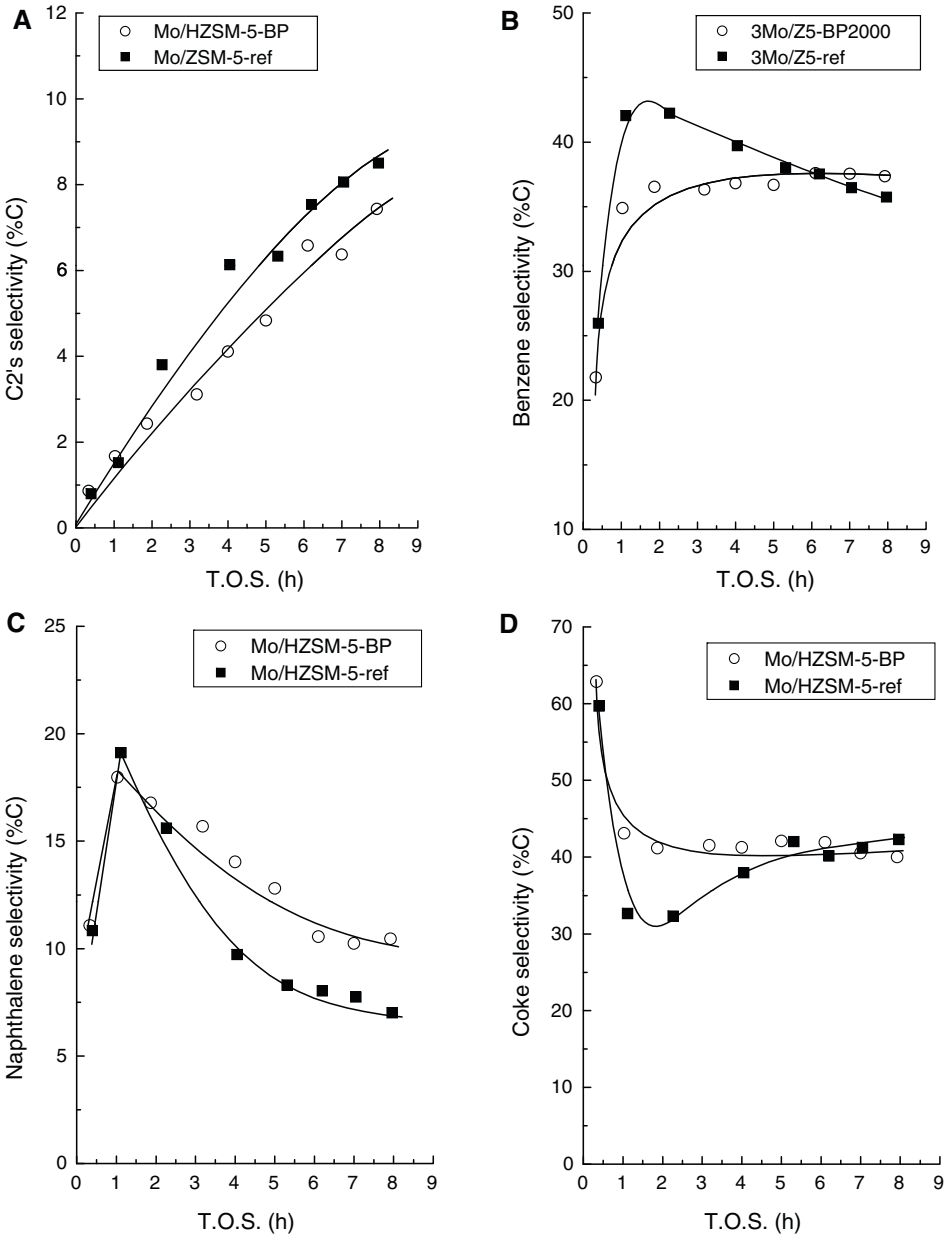

Fig. 6. Evolution with T.O.S. of the selectivities (%C) to the main reaction products formed during MDA on Mo/HZSM-5catalysts: (a) C_2 hydrocarbons (ethane + ethylene), (b) benzene, (c) naphthalene, (d) coke. Reaction conditions as in Fig. 5.

methane conversion is higher for the reference Mo/HZSM-5-ref catalyst. This fact can be ascribed to a higher amount of more active MoC_x nanoclusters which form upon carburization of Mo species that interacted with the zeolite Brønsted acid sites in the 10-ring channels, as it was indirectly inferred from the acidic and H_2-TPR characterizations discussed in the previous section. Very interestingly, it is observed in Fig. 5 that despite its lower initial activity, the carbon-templated Mo/HZSM-5-BP sample deactivates at a lower rate and gives a higher methane conversion than the reference catalyst for T.O.S. above 1–2 h. It is also quite remarkable that after the fast initial deactivation, the Mo/HZSM-5-BP catalyst reaches a *quasi*-steady state conversion level of ca. 5–6%, at least within the range of T.O.S. studied here, while the conversion gradually declines with T.O.S. for Mo/HZSM-5-ref, attaining a conversion value of around 4% after 8 h on stream. This result is somewhat surprising since for *conventional* Mo/HZSM-5 catalysts it has been reported that MoC_x nanoclusters located inside the channels (more abundant in the reference catalyst prepared here) are not only more active for methane activation, as indeed observed in Fig. 5, but also more stable during MDA [36]. In addition to this, one may consider that the higher residual Brønsted acidity of Mo/HZSM-5-BP (Table 2) could promote coke formation by catalyzing undesired condensation reactions of the primary aromatic products (predominantly benzene and naphthalene) that should accelerate catalyst deactivation. It appears, then, that the coke formed on Mo/HZSM-5-BP has a lower deactivating effect than that in Mo/HZSM-5-ref. It may be advanced that the better stability of Mo/HZSM-5-BP catalyst could be related in some way to the presence of the intracrystalline mesovoids in the carbon-templated zeolite. We will come back to this issue when discussing the amount and type of carbonaceous deposits present in the two catalysts after being used for 8 h in MDA reaction.

Fig. 6 shows the change in selectivity with T.O.S. for the main carbon-containing products, i.e. C_2, benzene, naphthalene, and coke. As it has been well documented in the previous literature, the selectivity to hydrocarbons at the very early stage of MDA (induc-

tion period) is very low and the main carbon-containing products are CO_x and coke coinciding with the carburization of MoO_x species by the reactant methane at the MDA reaction temperature [27]. In fact, as seen in Fig. 6d, initial (T.O.S. <0.5 h) coke selectivities around 60% (on a carbon basis) are obtained for the two catalysts. Coke selectivity rapidly drops during the first 1 h on stream while selectivity to aromatics is drastically increased during this initial period (Fig. 6b and c). Selectivity to C_2 hydrocarbons, mainly ethylene formed by coupling of methane on MoC_x species, continuously increases with T.O.S. (Fig. 6a). This trend reflects the gradual deactivation of the Brønsted acid sites of the HZSM-5 zeolite by coke deposits, which prevents further transformation of C_2 entities into the desired aromatics.

The selectivity results presented in Fig. 6 do reveal some interesting differences between Mo/HZSM-5-BP and Mo/HZSM-5-ref catalysts. For instance, C_2 selectivity is lower for Mo/HZSM-5-BP in the whole reaction period, suggesting that ethylene is more efficiently converted in this catalyst than in the reference one, the difference being more pronounced at increasing T.O.S. This suggests that a larger fraction of Brønsted acid sites remain active for catalyzing ethylene aromatization in Mo/HZSM-5-BP. Remarkable differences are also evidenced regarding benzene selectivity (Fig. 6b). In the case of Mo/HZSM-5-BP benzene selectivity initially increases and tends to reach a plateau at T.O.S. > 2 h (36–38% selectivity) while for Mo/HZSM-5-ref it passes through a maximum at T.O.S. = 1–2 h (42% selectivity) and then gradually declines with T.O.S. and attains lower values than for the carbon-templated catalyst above 6 h on stream. This trend further supports the better stability of Mo/HZSM-5-BP which was evidenced from the conversion-T.O.S. curves in Fig. 5. Regarding naphthalene selectivity, the other major aromatic product formed besides benzene (selectivity to toluene does not exceed 3% and 5% for Mo/HZSM-5-BP and Mo/HZSM-5-ref, respectively), it is seen in Fig. 6c that initially the two catalysts behave similarly reaching a maximum value of ca. 18–19% coinciding with the end of the induction period (T.O.S. ~ 1 h) and then declines with increasing T.O.S., the decrease being less pronounced for Mo/HZSM-5-BP. Despite naphthalene is thermodynamically favoured over benzene at the typical MDA temperatures (with a naphthalene/benzene ratio slightly above 1 at 700 °C), benzene is the main aromatic product formed on Mo/HZSM-5 catalysts due to the shape-selectivity imposed by the narrow 10-ring channels of the MFI structure. In this respect, it is commonly assumed that on *conventional* Mo/HZSM-5 naphthalene is predominantly formed at the acid sites on the external zeolite surface [40]. Taking into account that HZSM-5-ref has a lower average crystallite size than HZSM-5-BP (Table 1), and thus a larger external/internal surface ratio, it may be suggested that the higher naphthalene selectivity displayed by Mo/HZSM-5-BP in the post-induction period might be due to the contribution of the acid sites in the intracrystalline mesovoids to naphthalene formation under an unrestricted environment accompanied by a decreased path length for its diffusion from the mesovoids which are near the exterior of crystallites. At this point it should be recalled that a higher interconnection between 10-ring channels occurs due to the presence of intracrystalline mesovoids in HZSM-5-BP and this could also enhance the diffusion of bulky molecules through the crystallites contributing to the higher naphthalene selectivity observed for Mo/HZSM-5-BP. Finally, differences in the evolution of coke selectivity with T.O.S. are also evidenced in Fig. 6d. In the case of Mo/HZSM-5-ref, coke selectivity reaches a minimum of ca. 32% just after the induction period and then continuously increases with T.O.S. reaching a value of ca. 43% after 8 h on stream. By contrast, coke selectivity for Mo/HZSM-5-BP initially decreases and reaches a plateau at ca. 40% at T.O.S. > 2 h. It is evident from the area under the curves in Fig. 6d that the total amount of coke formed during the whole reaction period

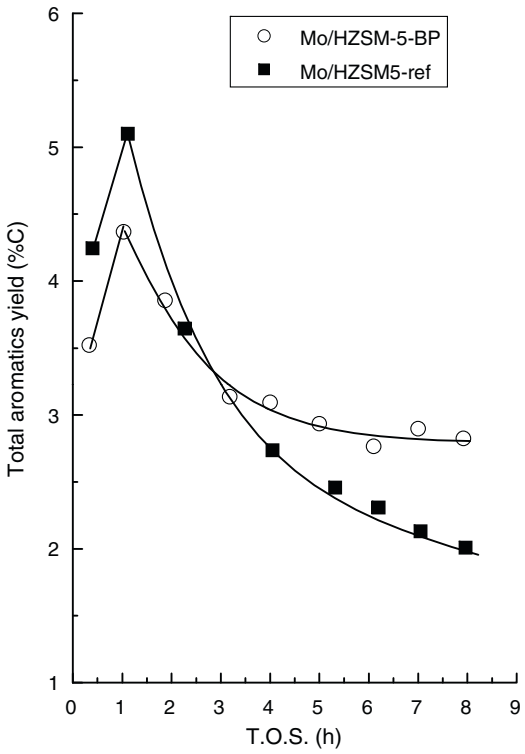

Fig. 7. Total aromatics yield as a function of T.O.S. Reaction conditions as in Fig. 5.

should be lower for the reference catalyst, as it will be confirmed in the following section. Moreover, even though the absolute coke selectivity values in the last reaction stages (5–8 h) do not differ much for the two catalysts, the fact that the selectivity remains almost constant with T.O.S. for Mo/HZSM-5-BP while it gradually increases for Mo/HZSM-5-ref in the post-induction period points toward a higher coke tolerance in the former catalyst containing the mesovoids. As a consequence, the catalyst comprising the carbon-templated zeolite gives a higher and more stable yield to the desired aromatics (C_6–C_{10}) than the reference catalyst, as clearly evidenced in Fig. 7. Thus, at a T.O.S. of 8 h the aromatics yield is about 2.8%C and 2.0%C for Mo/HZSM-5-BP and Mo/HZSM-5-ref, respectively, which represents an increment of 40% in relative terms.

3.4. Characterization of carbonaceous deposits

The amount and nature of the carbonaceous deposits formed on Mo/HZSM-5 catalysts after ca. 8 h on stream under MDA conditions have been studied by TG-DTG and TPO characterizations. The TGA curves shown in Fig. 8(left) reveal for both catalysts a substantial weight loss in the temperature range of 450–630 °C that corresponds to the burning-off of the coke deposits. The weight loss in that range is 6.2% for Mo/HZSM-5-BP and 4.5% for Mo/HZSM-5-ref reflecting a higher amount of carbonaceous deposits in the former. The small increase in weight observed below 450 °C (more apparent in the reference catalyst) is usually attributed to the oxidation of MoC_x species [41,42]. The derivative analysis of the TG curves (Fig. 8(right)) show, in the case of Mo/HZSM-5-BP, two well resolved peaks at ca. 490 °C and 565 °C due to the combustion of two different types of coke with distinct degrees of condensation (LT and HT coke, respectively). By contrast, only the low temperature combustion peak is clearly seen for Mo/HZSM-5-ref for which the high temperature feature becomes apparent as a shoulder. By combining the total amount of coke derived from the high temperature weight loss in the TG analyses with the relative proportion

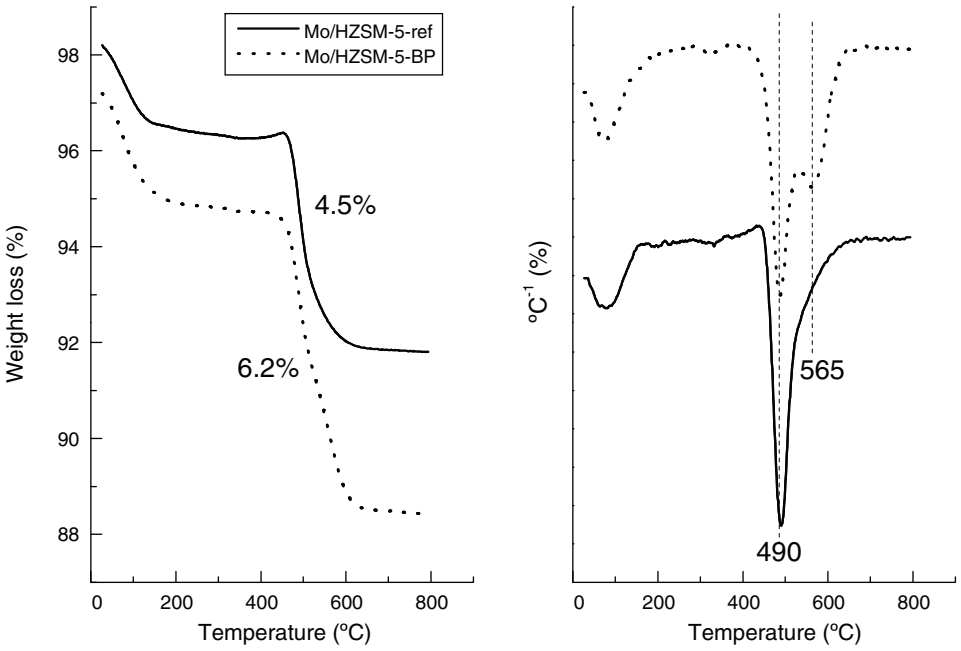

Fig. 8. TG (left) and DTG (right) analyses of coked Mo/HZSM-5 catalysts after being used for MDA during ca. 8 h.

of the two types of coke estimated from the relative areas of the two DTG peaks upon Gaussian deconvolution, the calculated weight percentages of LT and HT coke are 2.8% and 3.4% for Mo/HZSM-5-BP and 2.7% and 1.8% for Mo/HZSM-5-ref, respectively. Interestingly, while the amount of LT type coke is almost the same for the two catalysts (supporting the fact that it should be mostly associated with Mo species) that of HT coke is almost double for the carbon-templated catalyst. The coke present in spent catalysts has also been characterized by TPO. The corresponding CO_x ($CO + CO_2$) profiles are presented in Fig. 9. As observed, Mo/HZSM-5-ref displays a nearly single oxidation peak with a maximum at about 515 °C while Mo/HZSM-5-BP shows two features peaking at ca. 530 °C and 585 °C that should correspond with the LT and HT type coke, respectively, evidenced by TG-DTG analyses.

According to previous literature, the coke burnt at lower temperatures (LT-type) is formed on the Mo species, while that combusted at higher temperatures (HT coke) is mostly deposited on the zeolite Brønsted acid sites [21,43] and is believed to be the main responsible for the gradual catalyst deactivation during MDA. It is remarkable, however, that despite the higher amount of more deactivating HT-type coke formed on Mo/HZSM-5-BP it displayed a better stability with T.O.S. than the reference one during the MDA experiments, as discussed in the previous section. In order to explain this apparent contradiction, not only the acidity but also the porosity of the zeolite has to be considered. In this respect, it is evident that the mesovoids present in the interior of HZSM-5-BP crystallites may provide space enough for the growth and accumulation of coke deposits during MDA leading to the substantially higher amount of HT-type coke evidenced by TG-DTG and TPO results. While coke is being accumulated in the mesocavities, a larger fraction of Brønsted acid sites in the 10-ring channels would remain unpoisoned and thus active for aromatization for a longer period of time, as experimentally found here. It has also to be kept in mind that the intracrystalline mesovoids increase the interconnectivity between the 10-ring channels of the MFI zeolite and this might help in limiting the deleterious effect of the carbonaceous deposits in comparison to a *conventional* HZSM-5 zeolite. Then, we propose that the intracrystalline mesocavities in HZSM-5-BP may act as a trap for coke increasing the coke tolerance of the Mo/HZSM-5 catalyst and leading to the enhanced stability during the course of the MDA reaction. This mechanism is, in fact, similar to that previously proposed for the large 12-ring supercages of MCM-22 zeolite in order to account for the better tolerance to carbonaceous deposits and longer lifetime of Mo/HMCM-22 as compared with Mo/HZSM-5 [27].

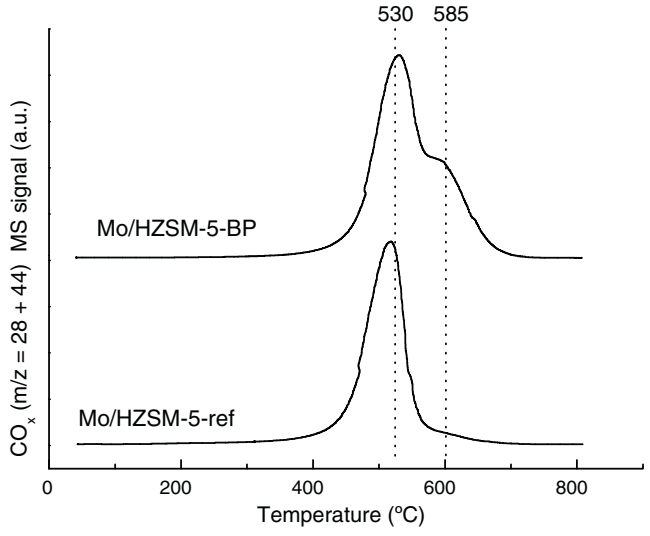

Fig. 9. $CO + CO_2$ profiles during TPO of coked Mo/HZSM-5 samples after being used for MDA during ca. 8 h.

4. Conclusions

In this work, a bifunctional Mo/HZSM-5-BP catalyst (3 wt% Mo, Si/Al = 26) has been prepared by using a hierarchical micro-mesoporous HZSM-5 sample synthesized in the presence of carbon nanoparticles. As ascertained by TEM, this zeolite contains intracrystalline mesovoids of ca. 10–20 nm in size formed upon combustion of the carbon template nanoparticles. For comparison purposes, a reference Mo/HZSM-5-ref sample with equivalent Mo loading and Si/Al ratio has also been prepared employing a com-

mercial zeolite (CBV5020, Zeolyst Int.). Both the carbon-templated and the commercial zeolite displayed an alike acidity in terms of acid type, density, and strength distribution (assessed by the combination of FTIR-pyridine and NH_3-TPD characterizations). After Mo loading and calcination at 500 °C, however, a larger fraction of Brønsted acid sites remained accessible to pyridine in Mo/HZSM-5-BP suggesting that the amount of Mo species that migrated and exchanged by protons inside the 10-ring pores (the precursors for the active MoC_x species) was lower in this catalyst as compared with the reference one. As a result, the initial methane conversion at typical MDA conditions (700 °C, 1 bar, 1500 ml/g_{cat} h) was also lower for Mo/HZSM-5-BP. However, it was interestingly found that the catalyst comprising the carbon-templated zeolite deactivated at a lower rate than the *conventional* catalyst resulting in a higher (40% relative increase at T.O.S. = 8 h) and stable aromatics yield. This occurred despite the fact that a larger amount of less reactive more condensed-type coke burning-off at high temperature formed on Mo/HZSM-5-BP, according to TG-DTG and TPO characterizations of spent catalysts. These results strongly point toward an improved coke tolerance accounting for the enhanced stability of the Mo/HZSM-5-BP catalyst with respect to that prepared from the commercial zeolite. We propose here that the better tolerance to carbonaceous deposits of Mo/HZSM-5-BP could be related to the presence of the intracrystalline mesopores acting as a trap for coke and allowing more coke to be formed while keeping a larger fraction of acid sites in the 10-ring channels active for aromatization.

Acknowledgements

Financial support by the Comisión Interministerial de Ciencia y Tecnología (CICYT) of Spain through the projects CTQ2007-66614/PPQ and CTQ2006-28341-E/BQU is gratefully acknowledged. Thanks are also due to the UE Network of Excellence IDECAT (FP6 Programme, NMP3-CT-2005-011730) which promoted the collaboration between the two research institutions.

Appendix A. Supplementary data

Supplementary data associated with this article can be found, in the online version, at doi:10.1016/j.cattod.2010.11.063.

References

[1] J.H. Lunsford, Catal. Today 63 (2000) 165–174.
[2] L. Wang, L. Tao, M. Xie, G. Xu, J. Huang, Y. Xu, Catal. Lett. 21 (1993) 35–41.
[3] K. Oshikawa, M. Nagai, S. Omi, J. Phys. Chem. B 105 (2001) 9124–9131.
[4] F. Solymosi, A. Szöke, J. Cserényi, Catal. Lett. 39 (1996) 157–161.
[5] Y. Xu, X. Bao, L. Lin, J. Catal. 216 (2003) 386–395.
[6] Y. Shu, H. Ma, R. Ohnishi, M. Ichikawa, Chem. Commun. (2003) 86–87.
[7] Y. Xu, L. Lin, Appl. Catal. A 188 (1999) 53–67.
[8] Y. Shu, M. Ichikawa, Catal. Today 71 (2001) 55–67.
[9] K. Skutil, M. Taniewski, Fuel Process. Technol. 87 (2006) 511–521.
[10] M. Guisnet, P. Magnoux, Appl. Catal. A 212 (2001) 83–96.
[11] S. Liu, L. Wang, Q. Dong, R. Ohnishi, M. Ichikawa, Chem. Commun. (1998) 1217–1218.
[12] H.S. Lacheen, E. Iglesia, J. Catal. 230 (2005) 173–185.
[13] S. Yuan, J. Li, Z. Hao, Z. Feng, Q. Xin, P. Ying, C. Li, Catal. Lett. 63 (1999) 73–77.
[14] S. Liu, R. Ohnishi, M. Ichikawa, J. Catal. 220 (2003) 57–65.
[15] L. Chen, L. Lin, Z. Xu, Catal. Lett. 39 (1996) 169–172.
[16] S. Liu, Q. Dong, R. Ohnishi, M. Ichikawa, Chem. Commun. (1997) 1455–1456.
[17] Y. Lu, D. Ma, Z. Xu, Z. Tian, X. Bao, L. Lin, Chem. Commun. (2001) 2048–2049.
[18] Y. Song, C. Sun, W. Shen, L. Lin, Catal. Lett. 109 (2006) 21–24.
[19] A. Martínez, E. Peris, A. Vidal-Moya, Stud. Surf. Sci. Catal. 174B (2008) 1075–1080.
[20] W. Ding, G.D. Meitzner, E. Iglesia, J. Catal. 206 (2002) 14–22.
[21] D. Ma, Y. Lu, L. Su, Z. Xu, Z. Tian, Y. Xu, L. Lin, X. Bao, J. Phys. Chem. B 106 (2002) 8524–8530.
[22] L. Su, L. Liu, J. Zhuang, H. Wang, Y. Li, W. Shen, Y. Xu, X. Bao, Catal. Lett. 91 (2003) 155–167.
[23] N. Chu, J. Yang, C. Li, J. Cui, Q. Zhao, X. Yin, J. Lu, J. Wang, Micropor. Mesopor. Mater. 118 (2009) 169–175.
[24] C.J.H. Jacobsen, C. Madsen, J. Houzvicka, I. Schimidt, A. Carlsson, J. Am. Chem. Soc. 122 (2000) 7116–7117.
[25] A. Burkat-Dulak, M. Derewinski, Stud. Surf. Sci. Catal. 174 (2008) 149–154.
[26] A. Martínez, M.A. Arribas, M. Derewinski, A. Burkat-Dulak, Appl. Catal. A 379 (2010) 188–197.
[27] D. Ma, Y. Shu, M. Cheng, Y. Xu, X. Bao, J. Catal. 194 (2000) 105–114.
[28] E.V. Matus, L.T. Tsykoza, Z.R. Ismagilov, V.V. Kuznetsov, Chem. Sustain. Dev. 11 (2003) 167–171.
[29] C.A. Emeis, J. Catal. 141 (1993) 347–354.
[30] W. Liu, Y. Xu, S. Song, L. Wang, J. Qin, N. Yang, J. Mol. Catal. A 120 (1997) 257–265.
[31] J.Z. Zhang, M.A. Long, R.F. Howe, Catal. Today 44 (1998) 293–300.
[32] H. Wang, L. Su, J. Zhuang, D. Tan, Y. Xu, X. Bao, J. Phys. Chem. B 107 (2003) 12972–12974.
[33] R.W. Borry III, Y.H. Kim, A. Huffsmith, J.A. Reimer, E. Iglesia, J. Phys. Chem. B 103 (1999) 5787–5796.
[34] L. Su, Y. Xu, X. Bao, J. Nat. Gas Chem. 11 (2002) 18–27.
[35] J.P. Tessonnier, B. Louis, S. Rigolet, M.J. Ledoux, C. Pham-Huu, Appl. Catal. A 336 (2008) 79–88.
[36] H. Liu, W. Shen, X. Bao, Y. Xu, Appl. Catal. A 295 (2005) 79–88.
[37] H. Zheng, D. Ma, X. Bao, J.A. Hu, J.H. Kwak, Y. Wang, C.H.F. Peden, J. Am. Chem. Soc. 130 (2008) 3722–3723.
[38] H. Liu, X. Bao, Y. Xu, J. Catal. 239 (2006) 441–450.
[39] Y. Song, C. Sun, W. Shen, L. Lin, Appl. Catal. A 317 (2007) 266–274.
[40] S. Kikuchi, R. Kojima, H. Ma, J. Bai, M. Ichikawa, J. Catal. 242 (2006) 349–356.
[41] H. Liu, L. Su, H. Wang, W. Shen, X. Bao, Y. Xu, Appl. Catal. A 236 (2002) 263–280.
[42] B.S. Liu, L. Jiang, H. Sun, C.T. Au, Appl. Surf. Sci. 253 (2007) 5092–5100.
[43] D. Ma, D.Z. Wang, L.L. Su, Y.Y. Shu, Y.D. Xu, X.H. Bao, J. Catal. 208 (2002) 260–269.